Journal of Power Sources 195 (2010) 8341–8346

Contents lists available at ScienceDirect

Journal of Power Sources

journal homepage: www.elsevier.com/locate/jpowsour

Short communication

Electrochemical performance of all-solid-state Li batteries based $LiMn_{0.5}Ni_{0.5}O_2$ cathode and NASICON-type electrolyte

J. Xie[a,*], N. Imanishi[b], T. Zhang[b], A. Hirano[b], Y. Takeda[b], O. Yamamoto[b], X.B. Zhao[a], G.S. Cao[a]

[a] Department of Materials Science and Engineering, Zhejiang University, Hangzhou 310027, China
[b] Department of Chemistry, Faculty of Engineering, Mie University, 1577 Kurimamachiya-cho, Tsu, Mie 514-8507, Japan

ARTICLE INFO

Article history:
Received 14 April 2010
Received in revised form 20 May 2010
Accepted 21 June 2010
Available online 1 July 2010

Keywords:
Lithium nickel manganese oxide
Glass ceramics electrolyte
All-solid-state lithium batteries
Cathode/electrolyte interface
Chemical diffusion coefficient

ABSTRACT

$LiNi_{0.5}Mn_{0.5}O_2$ thin films have been deposited on the NASICON-type glass ceramics, $Li_{1+x+y}Al_xTi_{2-x}Si_yP_{3-y}O_{12}$ (LATSP), by radio frequency (RF) magnetron sputtering followed by annealing. The films have been characterized by X-ray diffraction (XRD), scanning electron microscopy (SEM), and Raman spectroscopy. All-solid-state Li/PEO_{18}-$Li(CF_3SO_2)_2N$/LATSP/$LiNi_{0.5}Mn_{0.5}O_2$/Au cells are fabricated using the $LiNi_{0.5}Mn_{0.5}O_2$ thin films and the LATSP electrolyte. The electrochemical performance of the cells is investigated by galvanostatic cycling, cyclic voltammetry (CV), potentiostatic intermittent titration technique (PITT) and electrochemical impedance spectroscopy (EIS). Interfacial reactions between $LiNi_{0.5}Mn_{0.5}O_2$ and LATSP occur at a temperature as low as 300 °C with the formation of Mn_3O_4, resulting in an increased obstacle for Li-ion diffusion across the $LiNi_{0.5}Mn_{0.5}O_2$/LATSP interface. The electrochemical performance of the cells is limited by the interfacial resistance between LATSP and $LiNi_{0.5}Mn_{0.5}O_2$ as well as the Li-ion diffusion kinetics in $LiNi_{0.5}Mn_{0.5}O_2$ bulk.

1. Introduction

Since pioneered by Ohzuku et al. [1,2], $LiMn_{0.5}Ni_{0.5}O_2$ with a α-$NaFeO_2$ layered structure has been received great interest as a potential alternative cathode to $LiCoO_2$ due to its relatively lower cost and less toxicity compared with that of $LiCoO_2$. The material showed a high specific capacity of 200 mAh g^{-1} when cycled between 2.5 and 4.5 V with a good cycling stability [2]. In addition, this material also exhibited a better safety than $LiNiO_2$ and $LiMn_2O_4$ [2]. Furthermore, $LiMn_{0.5}Ni_{0.5}O_2$ shows little volume change during charge and discharge, guaranteeing close contact with the current collector when fabricating thin-film batteries and also close contact with the solid electrolyte when assembling all-solid-state batteries. Previous reports revealed that the $LiMn_{0.5}Ni_{0.5}O_2$ thin films had a good charge–discharge characteristic in the liquid electrolyte after annealed at high-temperature (over 700 °C) [3,4]. However, for the practical application of the films in all-solid-state thin-film batteries, some other factors should be taken into consideration, such as the Li-ion conductivity of the solid electrolyte and the interfacial stability between the cathode film and the solid electrolyte.

For the solid electrolyte, recently, an increasing attention has been paid to NASICON-type materials, because of their high Li-ion conductivity at room temperature [5–9]. The electrochemical cycling of all-solid-state Li-ion batteries based on NASICON-type electrolytes has been realized [10–15]. In addition to the search for suitable solid electrolytes, the chemical stability at the cathode/electrolyte interface is also an important factor, because post-annealing sometimes is necessary to optimize the electrochemical performance of the film. This annealing step, however, will generate undesirable side reactions between the cathode and the electrolyte, leading to the blocking of Li-ion diffusion passage [14,15]. Furthermore, the diffusion kinetics of Li-ion in bulk of the cathode film is another factor limiting its electrochemical performance. In our present work, $LiMn_{0.5}Ni_{0.5}O_2$ thin films were prepared by radio frequency (RF) magnetron sputtering on NASICON-type $Li_{1+x+y}Al_xTi_{2-x}Si_yP_{3-y}O_{12}$ (LATSP) solid electrolyte. All-solid-state Li/PEO_{18}-$Li(CF_3SO_2)_2N$/LATSP/$LiMn_{0.5}Ni_{0.5}O_2$/Au cells were fabricated to investigate the electrochemical performance of the films. Electrochemical impedance spectroscopy (EIS) and Li-ion chemical diffusion coefficients were measured in order to understand the intrinsic mechanism underlying the electrochemical performance of the all-solid-state batteries.

2. Experimental

The glass ceramics plates, LATSP (0.26 mm in thickness, OHARA Inc.), were used as the solid electrolyte for the following experiments. The $LiMn_{0.5}Ni_{0.5}O_2$ thin films (8 mm × 8 mm) were deposited on the LATSP substrates (10 mm × 10 mm) by RF mag-

* Corresponding author. Tel.: +86 571 87951203; fax: +86 571 87951451.
E-mail address: xiejian1977@zju.edu.cn (J. Xie).

0378-7753/$ – see front matter © 2010 Elsevier B.V. All rights reserved.
doi:10.1016/j.jpowsour.2010.06.066

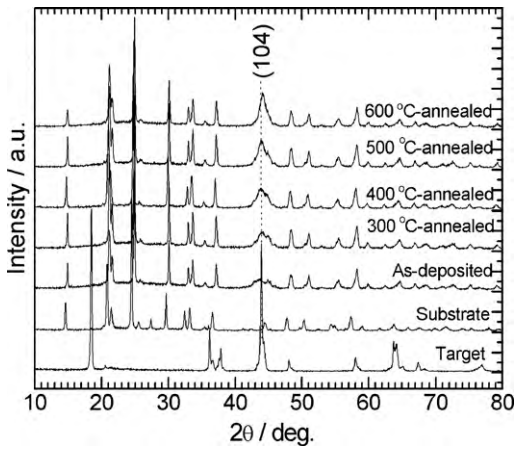

Fig. 1. XRD patterns of the $LiMn_{0.5}Ni_{0.5}O_2$ thin films on LATSP annealed at various temperatures.

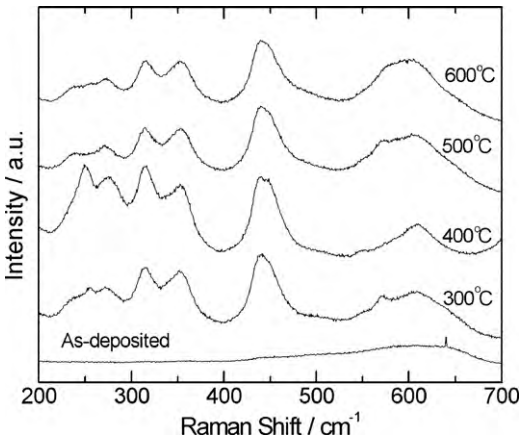

Fig. 2. Raman spectra of the $LiMn_{0.5}Ni_{0.5}O_2$ thin films on LATSP annealed at various temperatures.

netron sputtering using an Ulvac SCOTT-C3. The target used for sputtering was prepared by cold pressing $LiMn_{0.5}Ni_{0.5}O_2$ powder, prepared according to [16]. $LiMn_{0.5}Ni_{0.5}O_2$ sputtering was carried out in an Ar/O_2 mixture (30% O_2) with a total pressure of 2 Pa for 2 h. The as-deposited films were annealed at 300–600 °C for 30 min in air. Au was then deposited on the $LiMn_{0.5}Ni_{0.5}O_2$ by RF magnetron sputtering from an Au target for 30 min in pure Ar as the current collector. The crystalline structure of the as-deposited and the annealed films was characterized by X-ray diffraction (XRD) using a RINT2000/PC diffractometer with Cu Kα radiation and Raman spectra using a LabRamHRUV spectrometer. The surface and cross-sectional morphologies of the films were observed by scanning electron microscopy (SEM) using a Hitachi S-4800. The chemical composition of the film was determined by inductively coupled plasma (ICP) spectroscopy using a Shimadzu ICPS-1000IV spectrometer.

Li/PEO_{18}-$Li(CF_3SO_2)_2N$/LATSP/$LiMn_{0.5}Ni_{0.5}O_2$/Au cells were fabricated to investigate the electrochemical performance according to our previous report [14]. Galvanostatic cycling of the cells was carried out at various currents (5–100 μA) between 2.5 and 4.5 V at 50 °C. Cyclic voltammetry (CV) measurement was performed between 2.5 and 4.5 V at a scanning rate 0.1 mV s^{-1}. EIS measurement was conducted at 50–80 °C by applying an AC signal of 10 mV amplitude over the frequency range from 1 MHz to 1 mHz using a Solartron 1287 electrochemical interface combined with a Solartron 1260 frequency response analyzer. To investigate the interfacial resistances of Li/PEO_{18}-$Li(CF_3SO_2)_2N$ and PEO_{18}-$Li(CF_3SO_2)_2N$/LATSP in the Li/PEO_{18}-$Li(CF_3SO_2)_2N$/LATSP/$LiMn_{0.5}Ni_{0.5}O_2$/Au cell, two symmetric cells Li/PEO_{18}-$Li(CF_3SO_2)_2N$/Li and Li/PEO_{18}-$Li(CF_3SO_2)_2N$/LATSP/PEO_{18}-$Li(CF_3SO_2)_2N$/Li were fabricated and characterized by EIS at 50 °C. Li-ion chemical diffusion coefficient, $\tilde{D}_{Li}$, was measured by potentiostatic intermittent titration technique (PITT) at 50 °C in a voltage range of 3.6–4.3 V.

3. Results and discussion

Fig. 1 shows the XRD patterns of $LiMn_{0.5}Ni_{0.5}O_2$ thin films sputtered on LATSP annealed at various temperatures. Note that only a bump at around 45° (2θ) can be seen for the as-deposited $LiMn_{0.5}Ni_{0.5}O_2$ thin film, indicating that the film is amorphous or poorly crystallized. A broad peak appears when the film was annealed at 300 °C. With increasing the annealing temperature, the broad peak becomes sharp with its position shifted to a high angle, suggesting that $LiMn_{0.5}Ni_{0.5}O_2$ thin films on LATSP crystallized with a (1 0 4) preferred orientation. Our previous work showed that the same orientation was also observed for other two layered oxide thin films, $LiCoO_2$ [14] and $LiCo_{1/3}Mn_{1/3}Ni_{1/3}O_2$ [17], deposited also on LATSP. In contrast, the $LiMn_{0.5}Ni_{0.5}O_2$ thin films on Au and stainless steel showed a (0 0 3) preferred orientation [4]. This suggests that the film orientation is substrate dependent. The ICP analysis shows that the as-deposited film is Li-rich with a Li:Mn:Ni molar ratio of 2:0.766:0.766.

Fig. 2 shows the Raman spectra of the $LiMn_{0.5}Ni_{0.5}O_2$ thin films on LATSP annealed at different temperatures. Note that no obvious peak can be observed for the as-deposited film, indicative of the amorphous nature of the film, in agreement with the XRD results. After annealed at 300 °C for 30 min, two broad peaks at around and 450 and 600 cm^{-1} are evolved. The presence of this spectra band is characteristic of the layered $LiMn_{0.5}Ni_{0.5}O_2$ with a symmetry of R-3m [4,18]. The spectra band at 200–400 cm^{-1} can be attributed to Mn_3O_4 [19]. It is clear that Mn_3O_4 begins to form at a low temperature of 300 °C to form an inert layer. We did not find any Ni based compounds after annealing in Raman spectra and XRD patterns, which may due to that they are in an amorphous state and/or at a low amount.

Fig. 3 shows the SEM images of the 300 °C-annealed $LiMn_{0.5}Ni_{0.5}O_2$ thin film on LATSP. As seen in Fig. 3(a), the as-deposited film is composed of the irregular particles with a wide size distribution and the boundaries between the particles can be clearly seen. After annealing, the boundaries are not obvious and a leaf-like structure appears as seen in Fig. 3(b). It seems that the leaf-like structure comes from the part crystallization of the amorphous film. The thickness of the film is about be 1 μm after 2 h sputtering as shown in Fig. 3(c). Note that the film is dense and crack free. For the annealed film, however, the inert layer between LATSP and $LiMn_{0.5}Ni_{0.5}O_2$ is not clear. This may be due to that the inert layer is rather thin. As seen in Fig. 4, when the annealing is increased to 400 °C, the electrode exhibits a significant rise of resistance compared with the 300 °C-annealed one (see Fig. 7), which may serve as an indirect proof that the inert layer exists.

Fig. 5 compares the voltage profiles of the as-deposited and 300 °C-annealed $LiMn_{0.5}Ni_{0.5}O_2$ thin films. As seen in Fig. 5(a), the as-deposited film exhibits a low capacity and ill-defined potential plateaus, typical of materials with an amorphous state. In addition, the amorphous film shows a large irreversible capacity, which may be related to its Li-rich composition. For the 300 °C-annealed film, the potential plateaus are well developed with a significant reduction of the irreversible capacity as shown in Fig. 5(b), indicating improved crystallization and microstructural rearrangement of the film. However, the specific capacity of the film is below 100 mAh g^{-1}, rather lower than that of the well-crystallized mate-

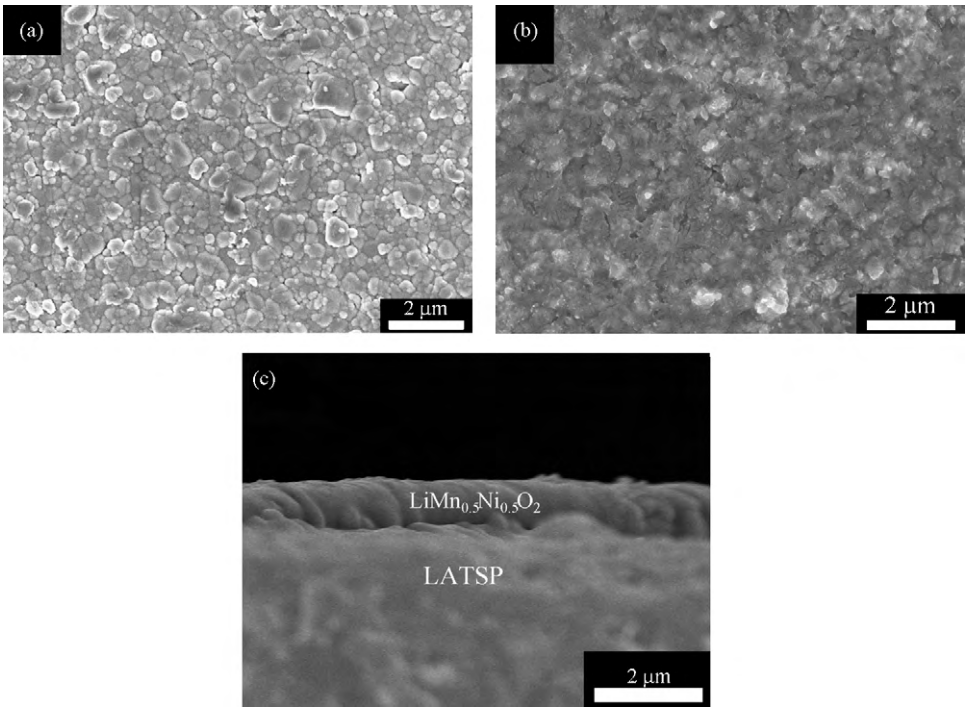

Fig. 3. SEM images of the $LiMn_{0.5}Ni_{0.5}O_2$ thin film on LATSP annealed at 300 °C: (a) surface and (b) cross section.

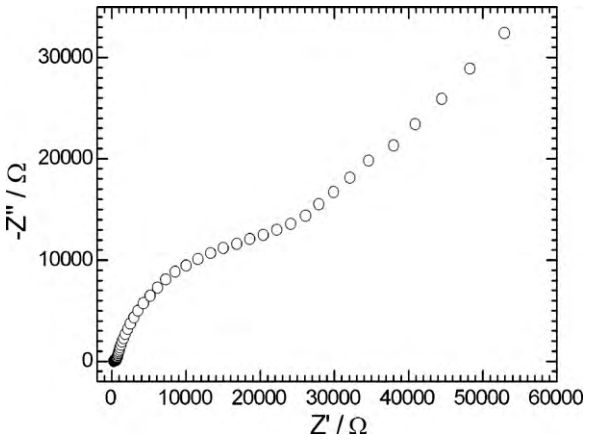

Fig. 4. Nyquist plot of the 400 °C-annealed $LiMn_{0.5}Ni_{0.5}O_2$ thin film on LATSP at 3.8 V measured at 50 °C.

rials prepared by high-temperature solid-phase reactions (in the similar cut-off voltage) [2,20]. A low reversible capacity of around 70 mAh g^{-1} was also observed for the all-solid-state lithium battery based on $LiMn_{0.5}Ni_{0.5}O_2$ cathode and superionic oxysulfide glass electrolyte [21]. It is suggested that the low specific capacity of our sample comes mainly from following factors: firstly, the film electrode has low electronic conductivity because it is conductive agent free; secondly, the Li-ion conductivity of presently used LATSP is in the order of 10^{-4} S cm^{-1} at room temperature [22], which is about 2 orders of magnitude lower than that of the commonly used liquid electrolytes, and the formation of the inert oxide layer after annealing increases the difficulty for Li-ion diffusion across the $LiMn_{0.5}Ni_{0.5}O_2$/LATSP interface; thirdly, the film is poorly crystallized and may exhibited a cation disordering between Li and Ni–Mn layer due to the low-temperature preparation process [23]. Further raising the annealing temperature will improve the crystallization of the film, but it also intensifies the interfacial reactions between $LiMn_{0.5}Ni_{0.5}O_2$ and LATSP. The electrochemical characterization on the high-temperature (over 400 °C) annealed samples showed that it gives rather low specific capacity and large polarization even at low current.

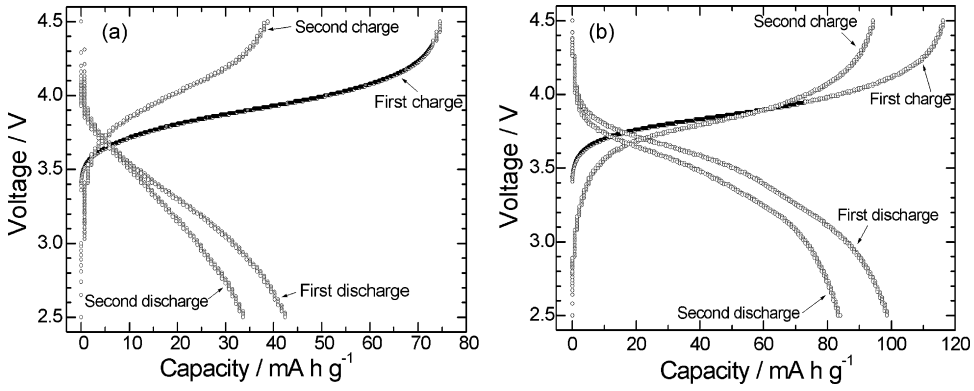

Fig. 5. Voltage profiles of the $LiMn_{0.5}Ni_{0.5}O_2$ thin films on LATSP: (a) as-deposited and (b) 300 °C-annealed, at a current of 5 μA.

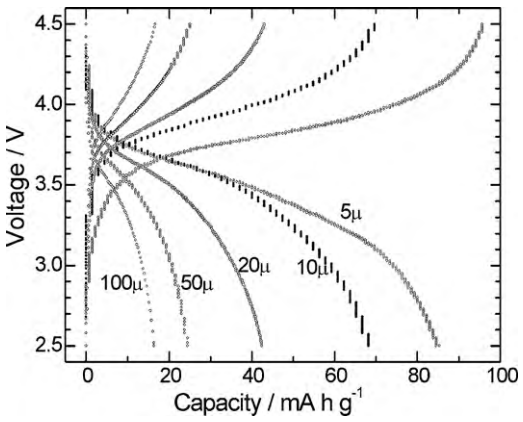

Fig. 6. Voltage profiles of the 300 °C-annealed $LiMn_{0.5}Ni_{0.5}O_2$ thin film on LATSP at various currents.

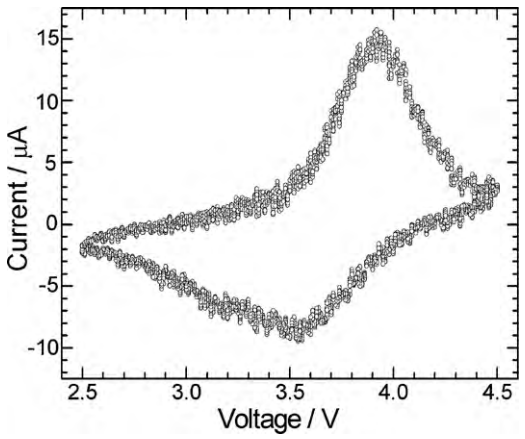

Fig. 7. CV plot of the 300 °C-annealed $LiMn_{0.5}Ni_{0.5}O_2$ thin film on LATSP at a scanning rate of 0.1 mV s^{-1}.

Fig. 6 shows the rate capability of the $LiMn_{0.5}Ni_{0.5}O_2$ thin film annealed at 300 °C. Note the film exhibits poor rate capability due to the limiting factors mentioned above. As seen in Fig. 7, the potential difference between cathodic and anodic peak in the CV plot is about 0.5 V, larger than that of the well-crystallized $LiMn_{0.5}Ni_{0.5}O_2$ thin film soaked by the liquid electrolyte [24,25], also suggesting a sluggish electrode kinetics of the all-solid-state battery.

EIS measurement was used to investigate the effect the Li-ion diffusion kinetics at the $LiMn_{0.5}Ni_{0.5}O_2$/LATSP interface on the electrochemical performance of the all-solid-state batteries. Fig. 8(a) shows typical Nyquist plots at 3.8 V in the temperature range 50–80 °C for the 300 °C-annealed $LiMn_{0.5}Ni_{0.5}O_2$ thin film. The Nyquist plot is composed of a slightly deformed semicircle in the high-frequency region and a sloping straight line in the low-frequency region. To separate each Li-ion diffusion process through the Li/PEO_{18}-$Li(CF_3SO_2)_2N$/LATSP/$LiMn_{0.5}Ni_{0.5}O_2$/Au cell, two symmetric cells, Li/PEO_{18}-$Li(CF_3SO_2)_2N$/Li and Li/PEO_{18}-$Li(CF_3SO_2)_2N$/LATSP/PEO_{18}-$Li(CF_3SO_2)_2N$/Li, were fabricated. Fig. 9 shows Nyquist plots of the two symmetric cells at 50 °C. Note that the resistance of the symmetric cell (for a single interface, only half value is considered) is rather smaller compared with that of the full cell. In addition, after the activation of the full cell by cycling, the interfacial resistances of Li/PEO_{18}-$Li(CF_3SO_2)_2N$ and PEO_{18}-$Li(CF_3SO_2)_2N$/LATSP in the full cell will be further reduced. Therefore, the above interfacial resistances can be ignored in the full cell. Thus, the semicircle in Fig. 8(a) corresponds to the Li-ion diffusion resistance, R_{ct}, through the $LiMn_{0.5}Ni_{0.5}O_2$/LATSP interface, and the straight line is related to the Li-ion diffusion in the $LiMn_{0.5}Ni_{0.5}O_2$ bulk. The temperature dependence of the interfacial

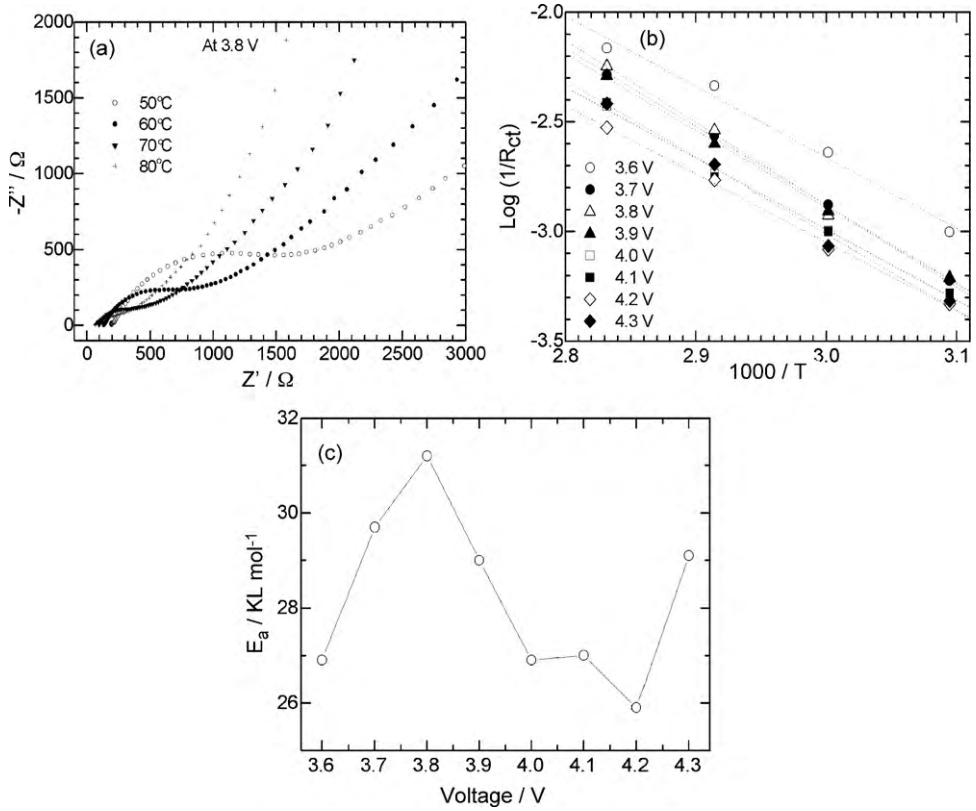

Fig. 8. EIS results of the 300 °C-annealed $LiMn_{0.5}Ni_{0.5}O_2$ thin film on LATSP: (a) Nyquist plots at 3.8 V measured at various temperatures, (b) temperature dependence of interfacial diffusion resistance, R_{ct}, at various voltages, and (c) voltage dependence of the activation energy for Li-ion interfacial diffusion.

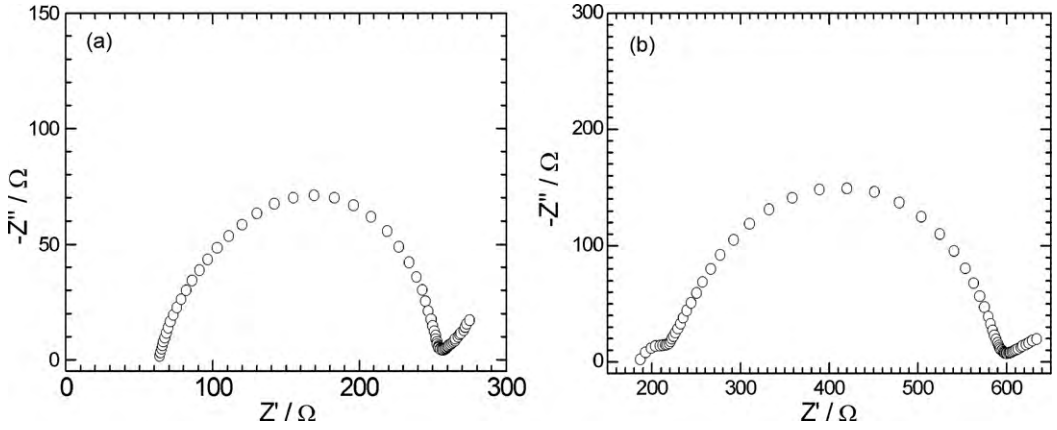

Fig. 9. Nyquist plots of two symmetric cells: (a) Li/PEO_{18}-Li(CF_3SO_2)$_2$N/Li and (b) Li/PEO_{18}-Li(CF_3SO_2)$_2$N/LATSP/PEO_{18}-Li(CF_3SO_2)$_2$N/Li.

diffusion resistance R_{ct} was investigated to understand the Li-ion interfacial diffusion kinetics. As shown in Fig. 8(b), a linear relationship between $\log(1/R_{ct})$ and $(1/T)$ can be observed at each voltage, indicating that the reciprocal diffusion resistance $(1/R_{ct})$ and the absolute temperature obeys the following Arrhenius equation:

$$\frac{1}{R_{ct}} = A \exp\left(\frac{-E_a}{RT}\right) \quad (1)$$

where E_a is the activation energy for Li-ion interfacial diffusion, T is the absolute temperature, R is the gas constant, R_{ct} is the Li-ion interfacial diffusion resistance, and A is the pre-exponential factor. The activation energy, E_a, can be calculated using the above equation and its voltage dependence is shown in Fig. 8(c). Note that the Li-ion diffusion resistance at the $LiMn_{0.5}Ni_{0.5}O_2$/LATSP interface is over 1000 Ω at 3.8 V (50 °C), significantly higher than that at the $LiMn_{0.5}Ni_{0.5}O_2$/liquid–electrolyte interface at the same voltage (only 50 Ω at room temperature for the freshly cycled cell) [26]. The large charge transfer resistance originates mainly from two factors: the one is the intrinsic low Li-ion conductivity of LATSP, and the other is inert oxide layer formed by the interfacial reactions upon annealing. As a result, the electrochemical performance of the all-solid-state batteries is limited by the large interfacial diffusion resistance. It is interesting to note that the activation energy for Li-ion diffusion through the $LiMn_{0.5}Ni_{0.5}O_2$/LATSP interface is smaller than those through $LiCoO_2$/$LiClO_4$-PC interface [27]. This may be due to the absence of the solid electrolyte interface (SEI) layer, which is formed in the case of using the liquid electrolyte, and/or due to the different diffusion mechanism.

Besides the diffusion at the $LiMn_{0.5}Ni_{0.5}O_2$/LATSP interface, the Li-ion diffusion in the $LiMn_{0.5}Ni_{0.5}O_2$ bulk also plays an important role in determining the electrochemical performance of the batteries. Therefore, the Li-ion chemical diffusion coefficients, $\tilde{D}_{Li}$, in the $LiMn_{0.5}Ni_{0.5}O_2$ thin films were measured using PITT method. Fig. 10 shows voltage dependence of the $\tilde{D}_{Li}$ values of the 300 °C-annealed film at 50 °C. As seen in the figure, the $\tilde{D}_{Li}$ values exhibit a continuous decrease with the increasing voltage. This means that the Li-ion extraction from the $Li_{1-x}Mn_{0.5}Ni_{0.5}O_2$ host becomes more and more difficult at a high x value, namely, a deep Li-deintercalation state. The $\tilde{D}_{Li}$ values of the $LiMn_{0.5}Ni_{0.5}O_2$ thin films on LATSP are about 3 orders of magnitude smaller than those of the $LiMn_{0.5}Ni_{0.5}O_2$ composite electrode (with binder and conductive agent) using the liquid electrolyte [26]. This may be due to the fact that Li-ion diffusion is facilitated by using the porous composite electrode soaked by the liquid electrolyte. Besides, $LiMn_{0.5}Ni_{0.5}O_2$ thin film prepared at a low temperature may show a cation disordering between Li and Ni–Mn layer that blocks the passages for Li-ion diffusion. As a result, the low $\tilde{D}_{Li}$ values of $LiMn_{0.5}Ni_{0.5}O_2$ thin film also contribute to its poor electrochemical performance.

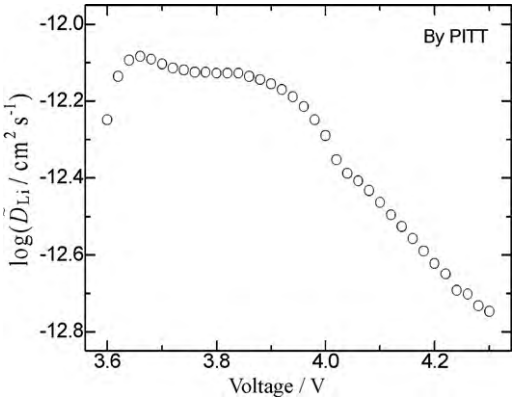

Fig. 10. Li-ion chemical diffusion coefficients in the 300 °C-annealed $LiMn_{0.5}Ni_{0.5}O_2$ thin film on LATSP.

4. Conclusions

$LiNi_{0.5}Mn_{0.5}O_2$ thin films, deposited on LATSP by RF magnetron sputtering, exhibited a (1 0 4) preferred orientation upon annealing. Interfacial reactions between $LiNi_{0.5}Mn_{0.5}O_2$ and LATSP begin to occur at a temperature as low as 300 °C to form Mn_3O_4. The formation of inert oxide layer increases the $LiNi_{0.5}Mn_{0.5}O_2$/LATSP interfacial resistance, blocking the Li-ion diffusion through the interface. This inert oxide layer together with the intrinsic low Li-ion conductivity leads to a poor electrochemical performance of the all-solid-state batteries. The Li-ion chemical diffusion coefficients in $LiNi_{0.5}Mn_{0.5}O_2$ thin film using solid electrolyte are rather smaller than those in $LiNi_{0.5}Mn_{0.5}O_2$ composite electrode using liquid electrolyte. As a result, the electrochemical performance of the Li/PEO_{18}-Li(CF_3SO_2)$_2$N/LATSP/$LiNi_{0.5}Mn_{0.5}O_2$/Au cells are limited by the above factors. The microstructures of both the thin film and its interface with the electrolyte should be optimized for the practical application in the all-solid-state thin-film batteries.

Acknowledgements

This research work was carried out under a collaboration program of Mie University and Genesis Research Institute, Nagoya, Japan. We thank OHARA Inc. for supplying the LATSP plates. We also thank the support of Zijin Program of Zhejiang University, China.

References

[1] T. Ohzuku, Y. Makimura, Chem. Lett. (2001) 744.
[2] Y. Makimura, T. Ohzuku, J. Power Sources 119–121 (2003) 156.

[3] S.J. Lai, C. Hu, Y.X. Li, D.B. Luo, M.H. Cao, Z.Y. Yu, H.X. Liu, Solid State Ionics 179 (2008) 1754.
[4] H. Xia, L. Lu, Appl. Phys. Lett. 92 (2008) 011912.
[5] J. Fu, Solid State Ionics 96 (1997) 195.
[6] J. Fu, J. Am. Ceram. Soc. 80 (1997) 1901.
[7] A.S. Best, P.J. Newman, D.R. MacFarlane, K.M. Nairn, S. Wong, M. Forsyth, Solid State Ionics 126 (1999) 191.
[8] K. Takada, M. Tansho, I. Yanase, T. Inada, A. Kajiyama, M. Kouguchi, S. Kondo, M. Watanabe, Solid State Ionics 139 (2001) 241.
[9] B. Kumar, D. Thomas, J. Kumar, J. Electrochem. Soc. 156 (2009) A506.
[10] K. Dokko, K. Hoshina, H. Nakano, K. Kanamura, J. Power Sources 174 (2007) 1100.
[11] K. Hoshina, K. Dokko, K. Kanamura, J. Electrochem. Soc. 152 (2005) A2138.
[12] Y. Iriyama, C. Yada, T. Abe, Z. Ogumi, K. Kikuchi, Electrochem. Commun. 8 (2006) 1287.
[13] C. Yada, Y. Iriyama, T. Abe, K. Kikuchi, Z. Ogumi, Electrochem. Commun. 11 (2009) 413.
[14] J. Xie, N. Imanishi, T. Zhang, A. Hirano, Y. Takeda, O. Yamamoto, J. Power Sources 189 (2009) 365.
[15] J. Xie, N. Imanishi, T. Zhang, A. Hirano, Y. Takeda, O. Yamamoto, J. Power Sources 192 (2009) 689.
[16] K.M. Shaju, G.V. Subba Rao, B.V.R. Chowdari, Electrochim. Acta 48 (2003) 1505.
[17] J. Xie, N. Imanishi, T. Zhang, A. Hirano, Y. Takeda, O. Yamamoto, J. Power Sources 195 (2010) 5780.
[18] S.W. Song, K.S. Han, H. Fujita, M. Yoshimura, Chem. Phys. Lett. 344 (2001) 299.
[19] T. Gao, H. Fjellvåg, P. Norby, Anal. Chim. Acta 648 (2009) 235.
[20] Z.H. Lu, L.Y. Beaulieu, R.A. Donaberger, C.L. Thomas, J.R. Dahn, J. Electrochem. Soc. 149 (2002) A778.
[21] F. Mizuno, A. Hayashi, K. Tadanaga, T. Minami, M. Tatsumisago, J. Power Sources 124 (2003) 170.
[22] T. Zhang, N. Imanishi, T. Zhang, S. Hasegawa, A. Hirano, J. Xie, Y. Takeda, O. Yamamoto, N. Sammes, J. Electrochem. Soc. 155 (2008) A965.
[23] M. Yoncheva, R. Stoyanova, E. Zhecheva, R. Alcantara, J.L. Tirado, J. Alloys Compd. 475 (2009) 96.
[24] H. Xia, L. Lu, M.O. Lai, Electrochim. Acta 54 (2009) 5986.
[25] D. Aurbach, B. Markovsky, G. Salitra, E. Markevich, Y. Talyossef, M. Koltypin, L. Nazar, B. Ellis, D. Kovacheva, J. Power Sources 165 (2007) 491.
[26] K.M. Shaju, G.V. Subba Rao, B.V.R. Chowdari, Electrochim. Acta 49 (2004) 1565.
[27] I. Yamada, Y. Iriyama, T. Abe, Z. Ogumi, J. Power Sources 172 (2007) 933.